

Detection and prebiotic chemistry of possible glycine precursor molecule methylenimine towards the hot molecular core G10.47+0.03

Arijit Manna¹ and Sabyasachi Pal¹

¹Department of Physics and Astronomy, Midnapore City College, Paschim Medinipur, India 721129

Abstract

Amino acids are essential for the synthesis of protein. Amino acids contain both amine (R-NH₂) and carboxylic acid (R-COOH) functional groups, which help to understand the possible formation mechanism of life in the universe. Among the 20 types of amino acids, glycine (NH₂CH₂COOH) is known as the simplest non-essential amino acid. In the last 40 years, all surveys of NH₂CH₂COOH in the interstellar medium, especially in the star-formation regions, have failed at the millimeter and sub-millimeter wavelengths. We aimed to identify the possible precursors of NH₂CH₂COOH, because it is highly challenging to identify NH₂CH₂COOH in the interstellar medium. Many laboratory experiments have suggested that methylenimine (CH₂NH) plays a key role as a possible precursor of NH₂CH₂COOH in the star-formation regions via the Strecker synthesis reaction. After spectral analysis using the local thermodynamic equilibrium (LTE) model, we successfully identified the rotational emission lines of CH₂NH towards the hot molecular core G10.47+0.03 using the Atacama Compact Array (ACA). The estimated column density of CH₂NH towards G10.47+0.03 is $(3.40 \pm 0.2) \times 10^{15}$ cm⁻² with a rotational temperature of 218.70 ± 20 K, which is estimated from the rotational diagram. The fractional abundance of CH₂NH with respect to H₂ towards G10.47+0.03 is 2.61×10^{-8} . We found that the derived abundance of CH₂NH agree fairly well with the existing two-phase warm-up chemical modelling abundance value of CH₂NH. We discuss the possible formation pathways of CH₂NH within the context of hot molecular cores, and we find that CH₂NH is likely mainly formed via neutral-neutral gas-phase reactions of CH₃ and NH radicals towards G10.47+0.03.

keywords: astrochemistry, Interstellar medium, prebiotic chemistry, star-formation region, millimeter astronomy

1. Introduction

At millimeter and submillimeter wavelengths, approximately 290 prebiotic and complex organic molecules have been discovered in the interstellar medium (ISM) or circumstellar shells^a. The identification of complex prebiotic molecules in the ISM is important to understand the chemical evolution of biologically relevant prebiotic molecules from fundamental molecular species (Herbst & van Dishoeck, 2009). Hot molecular cores are one of the early stages of high-mass star-formation regions (van Dishoeck & Blake, 1998; Herbst & van Dishoeck, 2009; Shimonishi et al., 2021; Manna et al., 2023; Manna & Pal, 2024a). The early stages of the high-mass star-formation regions are known as the chemically rich phase, which plays an essential role in understanding the formation of chemical complexity in the ISM (Tan et al., 2014; Shimonishi et al., 2021). In the hot molecular cores, the complex organic molecules escape from the icy surfaces of dust grains, or the complex organic molecules are created in the hot circumstellar gas (Herbst & van Dishoeck, 2009). Hot molecular cores are identified by their high gas density ($>10^6$ cm⁻³), small source size (<0.1 pc), and warm temperature (>100 K) (van Dishoeck & Blake, 1998; Kurtz et al., 2000). The warm-up time scale for hot molecular cores ranges from $\sim 10^4$ to $\sim 10^6$ years (van Dishoeck & Blake, 1998; Garrod et al., 2006; Garrod, 2013). The hot molecular phase is characterized by the rich molecular spectra of several complex organic molecules such as methanol (CH₃OH) and methyl cyanide (CH₃CN) (Allen et al., 2017). These complex molecules can form on the surface of dust grains on a cooler surface and are then released when the grains are heated owing to the formation of stars (Allen et al., 2017; Manna et al., 2023). Alternatively, these complex molecules may be created in massive young objects when the high temperature (>100 K) allows for endothermic reactions (Allen et al., 2017). Therefore, both formation pathways of complex organic molecules are important for acquiring molecular abundance around the hot molecular cores. Higher spectral and spatial resolution observations are required to identify the different complex organic molecules and the spatial distribution of these molecules in hot molecular cores. The detection of disc candidates in hot molecular cores is extremely rare, implying a link between the hot molecular core chemistry and discs (Allen et al., 2017). Studying the chemistry of the hot molecular cores of disc candidates can help us to understand the chemical evolution of high-mass star formations on small physical scales (Allen et al., 2017).

^a<https://cdms.astro.uni-koeln.de/classic/molecules>

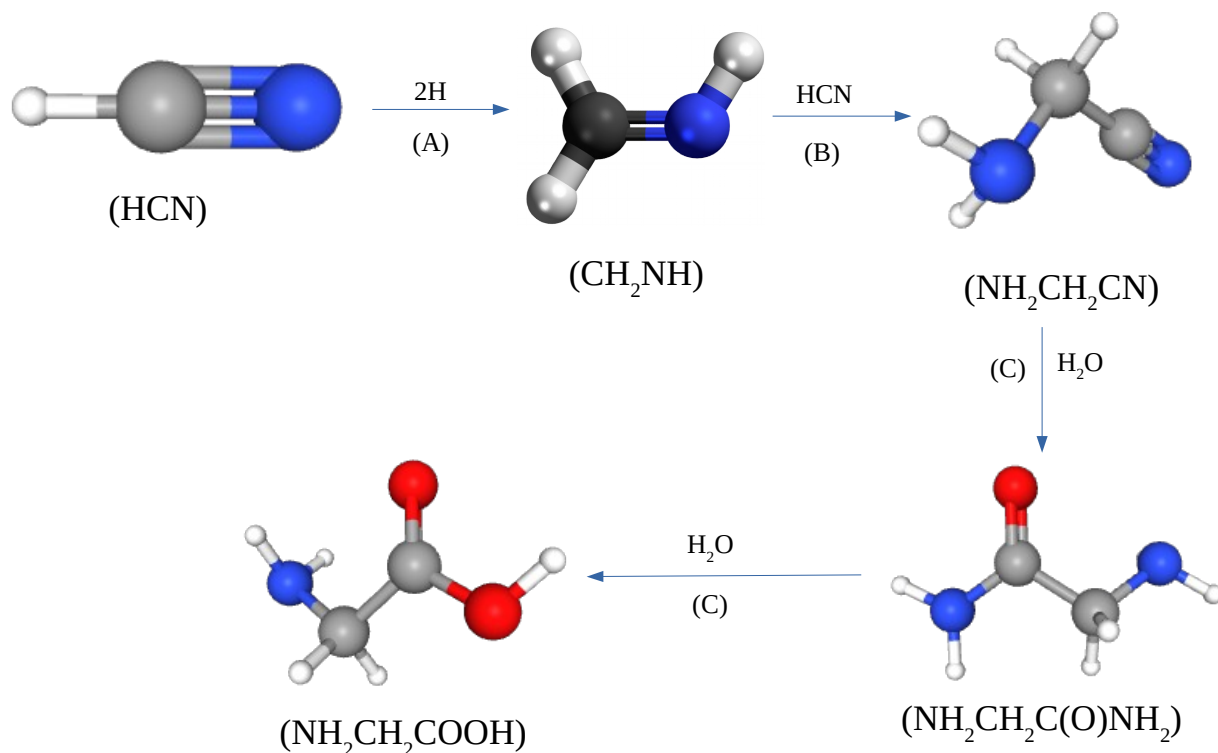


Fig. 1. Proposed possible formation mechanism of CH_2NH and $\text{NH}_2\text{CH}_2\text{COOH}$. In the chemical diagram, the black/grey dumbbell indicates the carbon (C) atom, the white dumbbell indicates the hydrogen (H) atom, the blue dumbbell indicates the nitrogen (N) atom, and the red dumbbell indicates the oxygen (O) atom. In the chemical reaction, “ H_2O ” represents the hydrolysis process. References: (A) Woon et al. (2002); Theule et al. (2011); (B) Danger et al. (2011); (C) Alonso et al. (2018).

The disc-like hot molecular core G10.47+0.03 is known as the ultra-compact (UC) H II region, which is located at a distance of 8.6 kpc with a luminosity of $5 \times 10^5 L_{\odot}$ (Cesaroni et al., 2010; Sanna et al., 2014). G10.47+0.03 is a disc-like candidate because, in this source, the hot core is embedded in the disc (Sanna et al., 2014; Manna & Pal, 2022a). Earlier, Rolfs et al. (2011) conducted a molecular spectral line survey of G10.47+0.03, using the Submillimeter Array (SMA) telescope in the frequency range of 199.9–692.2 GHz. Using the LTE modelling, Rolfs et al. (2011) detected the rotational emission lines of several simple and complex organic molecules such as sulfur monoxide (SO), sulfur dioxide (SO_2), cyanide (CN), hydrogen cyanide (HCN), hydrogen isocyanide (HNC), formamide (NH_2CHO), cyanoacetylene (HC_3N), vinyl cyanide ($\text{C}_2\text{H}_3\text{CN}$), formaldehyde (H_2CO), ethynol ($\text{H}_2\text{C}_2\text{O}$), ethanol ($\text{C}_2\text{H}_5\text{OH}$), dimethyl ether (CH_3OCH_3), methyl formate (CH_3OCHO), methanol (CH_3OH), and acetone (CH_3COCH_3) towards the G10.47+0.03. The rotational emission lines of methylamine (CH_3NH_2) and amino acetonitrile ($\text{NH}_2\text{CH}_2\text{CN}$) are also detected towards G10.47+0.03 (Ohishi et al., 2019; Manna & Pal, 2022a). The CH_3NH_2 and $\text{NH}_2\text{CH}_2\text{CN}$ molecules are known to be other possible precursors of the simplest amino acid, $\text{NH}_2\text{CH}_2\text{COOH}$, towards hot molecular cores. The emission lines of cyanamide (NH_2CN) and ethyl cyanide ($\text{C}_2\text{H}_5\text{CN}$) are detected from the hot molecular core G10.47+0.03 using ALMA (Manna & Pal, 2022b, 2023a). Recently, the rotational emission line of phosphorus nitride (PN) is detected towards the G10.47+0.03 (Manna & Pal, 2024b).

The asymmetric top-molecule methylenimine (CH_2NH) is known to be a possible precursor of $\text{NH}_2\text{CH}_2\text{COOH}$ in the ISM. The CH_2NH molecule was created by the hydrogenation of HCN on the dust surface of hot molecular cores (Woon et al., 2002; Theule et al., 2011). When CH_2NH and HCN both react with each other via the Strecker synthesis reaction, the complex amino and nitrile-bearing molecule amino acetonitrile ($\text{NH}_2\text{CH}_2\text{CN}$) is produced (Danger et al., 2011). The hydrolysis of $\text{NH}_2\text{CH}_2\text{CN}$ on the grain surface created glycnamide ($\text{NH}_2\text{CH}_2\text{C}(\text{O})\text{NH}_2$) (Alonso et al., 2018). Finally, $\text{NH}_2\text{CH}_2\text{COOH}$ can be created via hydrolysis of $\text{NH}_2\text{CH}_2\text{C}(\text{O})\text{NH}_2$ on the grain surface of hot molecular cores (Alonso et al., 2018). The proposed formation processes for CH_2NH and $\text{NH}_2\text{CH}_2\text{COOH}$ are shown in Figure 1. Earlier, Suzuki et al. (2016) claimed that the CH_2NH molecule is created in the gas phase between the reactions of CH_3 and NH ($\text{CH}_3 + \text{NH} \rightarrow \text{CH}_2\text{NH}$). Quantum chemical studies have shown that CH_3NH_2 is produced via the sequential hydrogenation of CH_2NH (Joshi & Lee, 2022). This indicates that both CH_2NH and CH_3NH_2 are chemically linked in ISM (Joshi & Lee, 2022). Subsequently, Garrod et al. (2022) confirmed that both CH_2NH and CH_3NH_2 are chemically linked towards hot molecular cores by using three-phase warm-up chemical models. Both Joshi & Lee (2022) and Garrod et al. (2022) showed that CH_3NH_2 and CH_2NH are chemically connected with $\text{NH}_2\text{CH}_2\text{COOH}$. Previously, many authors claimed that CH_2NH was detected in the high-mass star-formation region Sgr B2. Evidence of CH_2NH was found near Sgr B2 (OH) (Godfrey et al., 1973; Turner, 1989), Sgr B2 (N) (Halfen et al., 2013), and Sgr B2 (M) (Sutton et al., 1991). Previously, Jones et al. (2008, 2011) created the spatial distribution of CH_2NH from Sgr B2 (N) to Sgr B2 (S) at wavelengths of 3 and 7 mm using the MOPRA telescope. Belloche et al. (2013) demonstrated a detailed analysis of CH_2NH towards Sgr B2 (N) and Sgr B2 (M) using the IRAM 30 m telescope. The rotational emission lines of CH_2NH were also detected for W51 e1/e2, Orion KL, G34.3+0.15, G19.61-0.23, IRAS 16293–2422 B, and NGC 6334I (Dickens et al., 1997; White

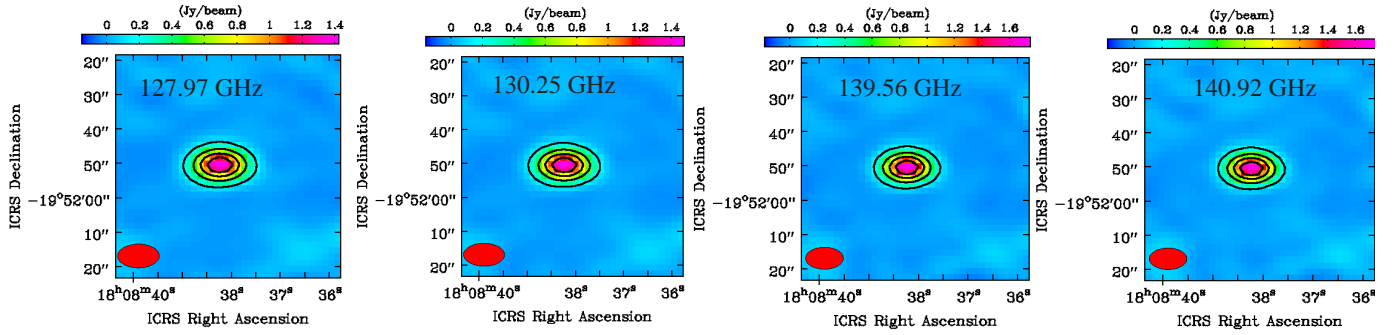


Fig. 2. Millimeter-wavelength continuum emission images of the hot molecular core G10.47+0.03. Continuum emission images are obtained with ACA band 4 at frequencies of 127.97 GHz, 130.25 GHz, 139.56 GHz, and 140.92 GHz. The contour levels start at 3σ , where σ is the RMS of each continuum image. The contour levels increase by a factor of $\sqrt{2}$. The red circles indicate the synthesized beams of the continuum images. The corresponding synthesized beam sizes and RMS values of all continuum images are presented in Table 1.

et al., 2003; Qin et al., 2010; Ligterink et al., 2018; Bøgelund et al., 2019). Recently, CH_2NH megamaser^b lines were detected in six compact obscured nuclei using the Very Large Array (VLA) (Gorski et al., 2021).

In this article, we present the identification of the possible $\text{NH}_2\text{CH}_2\text{COOH}$ precursor molecule CH_2NH towards G10.47+0.03, using ACA. To estimate the column density and rotational temperature of CH_2NH , we used a rotational diagram model. ACA observations and data reductions are presented in Section 2. The results of the detection of the emission lines of CH_2NH are presented in Section 3. The discussion and conclusion of the detection of CH_2NH are presented in Sections 4 and 5.

2. Observation and data reductions

We used the archival data of G10.47+0.03 in cycle 4, which was observed using the Atacama Compact Array (ACA) with a 7-m array (PI: Rivilla, Victor; ID: 2016.2.00005.S). The ACA is the heart of the Atacama Large Millimeter/submillimeter Array (ALMA). The observed phase centre of the hot molecular core G10.47+0.03 is $(\alpha, \delta)_{\text{J2000}} = 18:08:38.232, -19:51:50.400$. The observation was carried out on September 16, 2017, using 11 antennas. The observations were made with ACA band 4 with spectral ranges of 127.47–128.47 GHz, 129.74–130.74 GHz, 139.07–140.07 GHz, and 140.44–141.44 GHz and a corresponding spectral resolution of 488 kHz. During the observation, the flux calibrator and bandpass calibrator were J1924–2914, and the phase calibrator was J1833–210B.

For data reduction and imaging, we used the Common Astronomy Software Application (CASA 5.4.1) with an ALMA data reduction pipeline (McMullin et al., 2007). The data analysis flow chart is shown in Manna & Pal (2024c). For flux calibration using the flux calibrator, we used the Perley-Butler 2017 flux calibrator model for each baseline to scale the continuum flux density of the flux calibrator using the CASA task SETJY (Perley & Butler, 2017). We constructed the flux and bandpass calibration after flagging bad antenna data and channels using the CASA pipeline with tasks `hifa_bandpassflag` and `hifa_flagdata`. After the initial data reduction, we used the task MSTRANSFORM with all available rest frequencies to separate the target data of G10.47+0.03. For continuum and background subtraction, we used task UVCONTSUB in the UV plane of the separated calibrated data. We used the CASA task TCLEAN with a Briggs weighting robust value of 0.5, to create continuum and spectral images of the G10.47+0.03. To produce spectral images, we used the `SPECMODE = CUBE` parameter in the TCLEAN task. The final spatial resolution of the spectral data cubes was $10.48'' \times 6.28''$, $10.82'' \times 6.39''$, $12.08'' \times 6.90''$, and $12.08'' \times 6.79''$ between the frequency ranges of 127.47–128.47 GHz, 129.74–130.74 GHz, 139.07–140.07 GHz, and 140.44–141.44 GHz with a spectral resolution of 488.28 kHz. Finally, we used the CASA task IMPBCOR to correct the primary beam pattern in continuum images and spectral data cubes.

3. Result

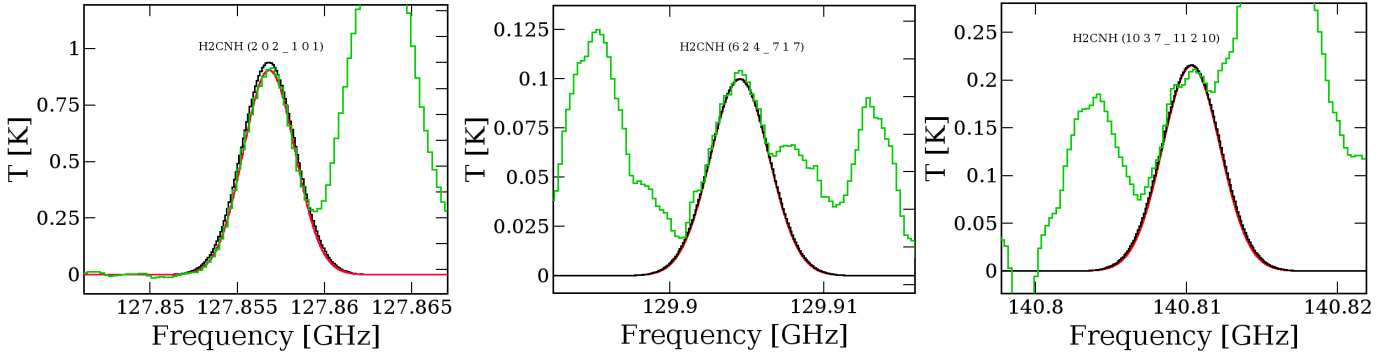
3.1 Continuum emission towards the G10.47+0.03

We presented the continuum emission images of the hot molecular core G10.47+0.03 at frequencies of 127.97 GHz, 130.25 GHz, 139.56 GHz, and 140.92 GHz. The continuum images are shown in Figure 2, where the surface brightness colour scale has units of the Jy beam^{-1} . After the creation of the continuum emission images, we fitted the 2D Gaussian over the continuum emission images using the CASA task IMFIT and estimated the integrated flux density in Jy, peak flux density in Jy beam^{-1} , synthesized beam size in arcsec ($''$), deconvolved beam size in arcsec ($''$), position angle in degrees ($^\circ$), and RMS in mJy of the hot core G10.47+0.03. The estimated continuum image properties of hot core G10.47+0.03 are shown in Table 1. We noticed that the continuum emission region of G10.47+0.03 is smaller than the synthesized beam size, which was estimated after fitting the 2D Gaussian over the continuum emission region. This indicates that the continuum emission image of G10.47+0.03 was not resolved between the frequency range of 127.97 GHz to 140.92 GHz. Recently, Manna & Pal (2023a) reported the detection of continuum emission from the G10.47+0.03 in the frequency range of 130.23 GHz–160.15 GHz with a flux density variation of 1.36–2.71 Jy.

^bA megamaser is a type of astrophysical maser in which the luminosities of the spectral lines are 100 million times brighter than normal masers emission lines in the ISM.

Table 1. Summary of the millimeter wavelength continuum images of G10.47+0.03.

Frequency (GHz)	Wavelength (mm)	Integrated flux (Jy)	Peak flux (Jy beam ⁻¹)	Beam size (″×″)	Deconvolved source size (″×″)	RMS (mJy)	Position angle (°)
127.97	2.34	1.57±0.01	1.44±0.08	12.02×6.87	2.60×2.18	9.16	-89.71
130.25	2.30	1.66±0.01	1.51±0.08	11.96×6.73	2.73×2.52	8.76	-89.63
139.56	2.14	1.98±0.02	1.78±0.01	10.73×6.35	2.71×2.29	10.72	-89.61
140.92	2.12	2.00±0.02	1.78±0.01	10.61×6.25	2.75×2.44	11.68	-89.91

**Fig. 3.** Identified rotational emission lines of CH₂NH towards the G10.47+0.03 in the frequency ranges of 127.47–128.47 GHz, 129.74–130.74 GHz, and 140.44–141.44 GHz. The green spectra indicate the millimeter-wavelength molecular spectra of G10.47+0.03. The black spectra present the best-fit LTE model spectra of CH₂NH, and the red spectra indicate the Gaussian model. The radial velocity of the spectra is 68.50 km s⁻¹.

3.2 Identification of the CH₂NH in the G10.47+0.03

First, we extracted the millimeter-wavelength molecular spectra from the spectral data cubes to create a 23.75″ diameter circular region over the G10.47+0.03. The synthesized beam sizes of the spectral data cubes of hot core G10.47+0.03 is 10.48″×6.28″, 10.82″×6.39″, 12.08″×6.90″, and 12.08″×6.79″. Hot core G10.47+0.03 is located at a distance of 8.6 kpc and at that distance, a ∼10″ resolution refers to a spatial scale of 0.4 pc. This implies that the extracted spectrum mostly represents the outer envelope. The systematic velocity (V_{LSR}) of G10.47+0.03 is 68.50 km s⁻¹ (Rolffs et al., 2011). We used the second-order polynomial to subtract the baseline of the entire spectra. To identify the rotational emission lines of CH₂NH, we used the local thermodynamic equilibrium (LTE) model with the Cologne Database for Molecular Spectroscopy (CDMS) database (Müller et al., 2005). For LTE modelling, we used CASSIS (Vastel et al., 2015). The LTE assumptions are valid in the inner region of G10.47+0.03 because the gas density of the warm inner region of the hot core was 7×10^7 cm⁻³ (Rolffs et al., 2011). To fit the LTE model spectra of CH₂NH over the millimeter wavelength spectra of G10.47+0.03, we applied the Markov Chain Monte Carlo (MCMC) algorithm in CASSIS. After the LTE analysis, we have detected a total of three transitions of CH₂NH i.e., $J = 2(0,2) - 1(0,1)$, $J = 6(2,4) - 7(1,7)$, and $J = 10(3,7) - 11(2,10)$. The three detected transitions of CH₂NH had hyperfine lines. We do not discuss the hyperfine lines regarding the identified transitions of CH₂NH because the current spectral resolution is insufficient to resolve the hyperfine lines. The CH₂NH is a simple asymmetric top with all atoms being on the simple plane, and the transitions are described using labels of J' , K'_p , K'_o , and J'' , K''_p , K''_o . In the transition of CH₂NH, J indicated the total rotational angular momentum quantum number, K_p indicated the projection of J on the symmetry axis in the limiting prolate symmetric top, K_o indicated the projection of J on the symmetry axis in the limiting oblate symmetric top, and F indicated the total angular momentum quantum number, which includes the nuclear spin for the nucleus with the largest χ or eQq where χ or eQq denoted the nuclear electric quadrupole coupling constant along the indicated principal axis (Kirchhoff et al., 1973). There were no missing transitions of CH₂NH in the observable frequency ranges. As per the CDMS and online molecular database Splatalogue, we find that all the detected transitions of CH₂NH are not blended with other nearby molecular transitions. Using the LTE model, the best-fit column density of CH₂NH was $(3.21 \pm 1.5) \times 10^{15}$ cm⁻² with an excitation temperature of 210.50 ± 32.82 K and a source size of 10.78″. The full-width half maximum (FWHM) of the LTE-fitted rotational emission spectra of CH₂NH was 9.5 km s⁻¹. The LTE-fitted rotational emission spectra of CH₂NH are shown in Figure 3. After identifying the rotational emission lines of CH₂NH using the LTE model, we obtained the molecular transitions, upper-state energy (E_u) in K, Einstein coefficients (A_{ij}) in s⁻¹, line intensity ($S\mu^2$) in Debye², and optical depth (τ). We also verified the detected transitions of CH₂NH from Kirchhoff et al. (1973). To estimate the proper FWHM and integrated intensity ($\int T_{mb} dv$) of the detected emission lines of CH₂NH, we fitted a Gaussian model to the observed spectra of CH₂NH. A summary of the detected transitions and spectral line properties of CH₂NH are presented in Table 2.

3.3 Rotational diagram analysis of CH₂NH

In this work, we used the rotational diagram method to estimate the total column density (N) in cm⁻² and the rotational temperature (T_{rot}) in K of CH₂NH because we detected multiple transition lines of CH₂NH towards G10.47+0.03. Initially, we assumed that

Table 2. Summary of the molecular line parameters of the CH₂NH towards the G10.47+0.03

Frequency (GHz)	Transition*	E_u^Δ (K)	A_{ij}^Δ (s ⁻¹)	g_{up}^Δ	$S\mu^{2\dagger}$ (Debye ²)	FWHM [‡] (km s ⁻¹)	$\int T_{mb} dV^\ddagger$ (K km s ⁻¹)	Optical depth (τ)
127.856	2(0,2)–1(0,1)	9.21	1.75×10^{-5}	15	10.76	9.49 ± 0.10	5.97 ± 0.25	2.96×10^{-4}
129.904	6(2,4)–7(1,7)	96.38	3.23×10^{-6}	39	4.93	9.62 ± 0.48	0.61 ± 0.06	4.87×10^{-4}
140.810	10(3,7)–11(2,10)	240.27	4.85×10^{-6}	63	9.41	9.56 ± 0.98	0.23 ± 0.09	8.51×10^{-4}

*–All detected transitions of CH₂NH are also verified from Table 2 in Kirchoff et al. (1973) and CDMS molecular database.

Δ –The values of E_u , A_{ij} and g_{up} are taken from the CDMS database.

\dagger –The line intensity $S\mu^2$ is defined by the product of the transition line strength S and square of the dipole moment μ^2 of CH₂NH. The values of $S\mu^2$ of detected transitions of CH₂NH are taken from online molecular database [splatalogue](#).

\ddagger –FWHM and $\int T_{mb} dV$ are estimated from the fitting of the Gaussian model over the observed spectra of CH₂NH

the detected CH₂NH emission lines were optically thin and populated under the LTE conditions. The equation of column density for optically thin molecular emission lines can be expressed as (Goldsmith & Langer, 1999),

$$N_u^{thin} = \frac{3g_u k_B \int T_{mb} dV}{8\pi^3 \nu S \mu^2} \quad (1)$$

where g_u is the degeneracy of the upper state, μ is the electric dipole moment, S indicates the strength of the transition lines, ν is the rest frequency, k_B is Boltzmann's constant, and $\int T_{mb} dV$ indicates the integrated intensity. The total column density of CH₂NH under LTE conditions can be written as,

$$\frac{N_u^{thin}}{g_u} = \frac{N_{total}}{Q(T_{rot})} \exp(-E_u/k_B T_{rot}) \quad (2)$$

where E_u is the upper-state energy of CH₂NH, T_{rot} is the rotational temperature of CH₂NH, and $Q(T_{rot})$ is the partition function at the extracted rotational temperature. The rotational partition function of CH₂NH at 75 K is 740.457, that at 150 K is 2084.970, and that at 300 K is 5892.504 (Müller et al., 2005). Equation 2 can be rearranged as,

$$\ln\left(\frac{N_u^{thin}}{g_u}\right) = \ln(N) - \ln(Q) - \left(\frac{E_u}{k_B T_{rot}}\right) \quad (3)$$

Equation 3 indicates a linear relationship between the upper state energy (E_u) and $\ln(N_u/g_u)$ of CH₂NH. The value $\ln(N_u/g_u)$ was estimated using Equation 1. Equation 3 indicates that the spectral parameters with respect to the different transition lines of CH₂NH should be fitted with a straight line, whose slope is inversely proportional to the rotational temperature (T_{rot}), with its intercept yielding $\ln(N/Q)$, which will help estimate the molecular column density of CH₂NH. For the rotational diagram analysis, we estimated the spectral line parameters of CH₂NH after fitting the Gaussian model over the observed spectra of CH₂NH using the Levenberg-Marquardt algorithm in CASSIS (see Section 3.2 for details on spectral fitting). For the rotational diagram analysis, we used all the detected transitions of CH₂NH to estimate the accurate column density and rotational temperature because all the detected transitions of CH₂NH are non-blended. The resultant rotational diagram of CH₂NH is shown in Figure 4, which was created using the ROTATIONAL DIAGRAM module in CASSIS. In the rotational diagram, the vertical red error bars indicate the absolute uncertainty of $\ln(N_u/g_u)$, which was determined from the estimated error of $\int T_{mb} dV$. From the rotational diagram, we estimated the column density of CH₂NH to be $(3.40 \pm 0.2) \times 10^{15}$ cm⁻² with a rotational temperature of 218.70 ± 20 K. From the LTE spectral modelling, we found that the column density and excitation temperature of CH₂NH are $(3.21 \pm 1.5) \times 10^{15}$ cm⁻² and 210.50 ± 32.82 K, which are nearly similar to the estimated column density and rotational temperature of CH₂NH using the rotational diagram model. Our derived rotational temperature of CH₂NH indicates that the detected transitions of CH₂NH arise from the warm-inner region of G10.47+0.03 because the temperature of the hot molecular core is above ≥ 100 K (van Dishoeck & Blake, 1998). To determine the fractional abundance of CH₂NH, we use the column density of CH₂NH inside the 12.08'' beam and divide it by the column density of H₂. The estimated fractional abundance of CH₂NH towards G10.47+0.03 with respect to H₂ was 2.61×10^{-8} , where the column density of H₂ towards G10.47+0.03 was 1.30×10^{23} cm⁻² (Suzuki et al., 2016).

3.4 Spatial distribution of CH₂NH in the G10.47+0.03

We created integrated emission maps of CH₂NH towards G10.47+0.03, using the CASA task IMMOMENTS. Integrated emission maps of CH₂NH were created by integrating the spectral data cubes in the velocity ranges of 61.06–74.11 km s⁻¹, 63.80–75.28 km s⁻¹, and 64.40–70.93 km s⁻¹, where the emission lines of CH₂NH were detected. We created integrated emission maps for the three non-blended transitions of CH₂NH towards G10.47+0.03. The integrated emission maps of CH₂NH with different transitions towards G10.47+0.03 are shown in Figure 5. The resultant integrated emission maps of CH₂NH were overlaid with the 2.34 mm continuum emission map of G10.47+0.03. The integrated emission maps of CH₂NH exhibit a peak at the continuum position. From the integrated emission maps,

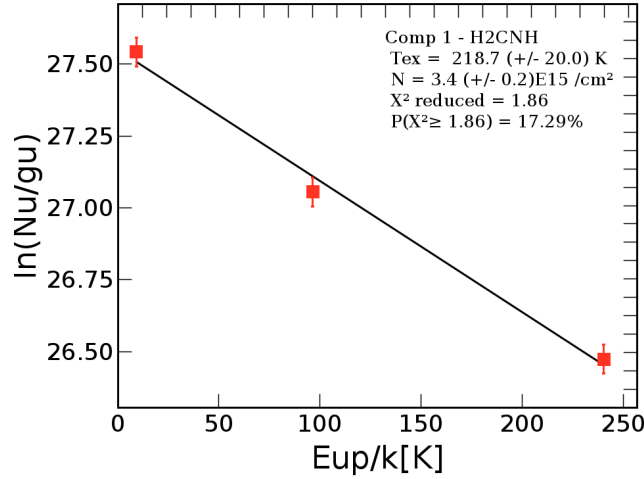


Fig. 4. Rotational diagram of CH₂NH towards G10.47+0.03. In the rotational diagram, the red blocks represent the statistical data points of all detected transitions, and the solid black line indicates the fitted straight line, which helps estimate the column density and rotational temperature of CH₂NH.

it is evident that the transitions of the CH₂NH molecule arise from the warm inner part of the hot core region of G10.47+0.03. This indicates that the temperature of the detected transition lines of CH₂NH is above 100 K because the temperature of the hot core ≥ 100 K (van Dishoeck & Blake, 1998). From the rotational diagram, we estimate the temperature of CH₂NH is 218.7 ± 20 K, which indicates the emission lines of CH₂NH arise from the warm-inner region of G10.47+0.03. After the generation of the integrated emission maps of all identified lines of CH₂NH, we estimated the emitting regions of CH₂NH towards G10.47+0.03 by fitting the 2D Gaussian over the integrated emission maps of CH₂NH using the CASA task IMFIT. The deconvolved beam size of the emitting region of CH₂NH was estimated by the following equation,

$$\theta_S = \sqrt{\theta_{50}^2 - \theta_{beam}^2} \quad (4)$$

where $\theta_{50} = 2\sqrt{A/\pi}$ indicates the diameter of the circle whose area (A) corresponds to the 50% line peak of CH₂NH and θ_{beam} is the half-power width of the synthesized beam (Rivilla et al., 2017; Manna & Pal, 2022c, 2023b). The estimated emitting regions of the $J = 2(0,2)-1(0,1)$, $J = 6(2,4)-7(1,7)$, and $J = 10(3,7)-11(2,10)$ transitions of CH₂NH were $10.520''$ (0.44 pc), $10.275''$ (0.430 pc), and $10.781''$ (0.451 pc). The emitting region of CH₂NH varied between $10.520''$ and $10.781''$. We observed that the emitting regions of CH₂NH were similar or small with respect to the synthesized beam size of the integrated emission maps, which means that the transition lines of CH₂NH were not spatially resolved or, at best, marginally resolved. Therefore, we cannot draw any conclusions about the morphology of the integrated emission maps of CH₂NH towards G10.47+0.03. Higher spectral resolution observations were needed using the ALMA 12 m array to solve the spatial distribution morphology of CH₂NH towards the hot molecular core G10.47+0.03.

4. Discussion

4.1. CH₂NH towards the G10.47+0.03

We presented the first interferometric detection of possible NH₂CH₂COOH precursor molecule CH₂NH towards the G10.47+0.03 using the ACA band 4. We identified a total of three transition lines of CH₂NH towards G10.47+0.03, and after spectral analysis using the LTE model, we observed that all identified transitions of CH₂NH are non-blended. Subsequently, these non-blended transition lines were used for rotational diagram analysis to estimate the total column density and rotational temperature of CH₂NH. Earlier, Suzuki et al. (2016) first attempted to search the rotational emission lines of CH₂NH from G10.47+0.03 and other hot molecular core objects. Suzuki et al. (2016) identified three transition lines of CH₂NH i.e., $J = 4(0,4)-3(1,3)$, $J = 4(1,4)-3(1,3)$, and $J = 4(2,3)-3(2,2)$ towards the G10.47+0.03 using the Nobeyama Radio Observatory (NRO) 45 m single dish telescope. Many questions arise in the detection of CH₂NH towards G10.47+0.03 by Suzuki et al. (2016). First, all detected spectral lines of CH₂NH towards G10.47+0.03 were below 2.5σ statistical significance (for details, see Figure 3 in Suzuki et al. (2016)), and the authors did not use any radiative transfer model for spectral characterization of CH₂NH. Suzuki et al. (2016) also did not discuss the blending effect of CH₂NH with nearby molecular transitions in the molecular spectra of G10.47+0.03. The single-dish observation of CH₂NH by Suzuki et al. (2016) could not study the spatial distribution of CH₂NH towards G10.47+0.03. Thus, Suzuki et al. (2016) did not estimate any information regarding the source size or emitting region of CH₂NH, which restricted the accuracy of their measurements of the proper column density of the detected molecules. We also observed that the upper state energy (E_u) of the transition lines of CH₂NH detected by Suzuki et al. (2016) varies between 10 and 30 K. In the rotational diagram, lower energy levels will not enable accurate determination of the column density. In the rotational diagram, transitions at significantly higher energy levels can determine a more accurate column density. Our interferometric detection of CH₂NH using ACA gives us confidence in the more accurate column density of CH₂NH because the upper state energies

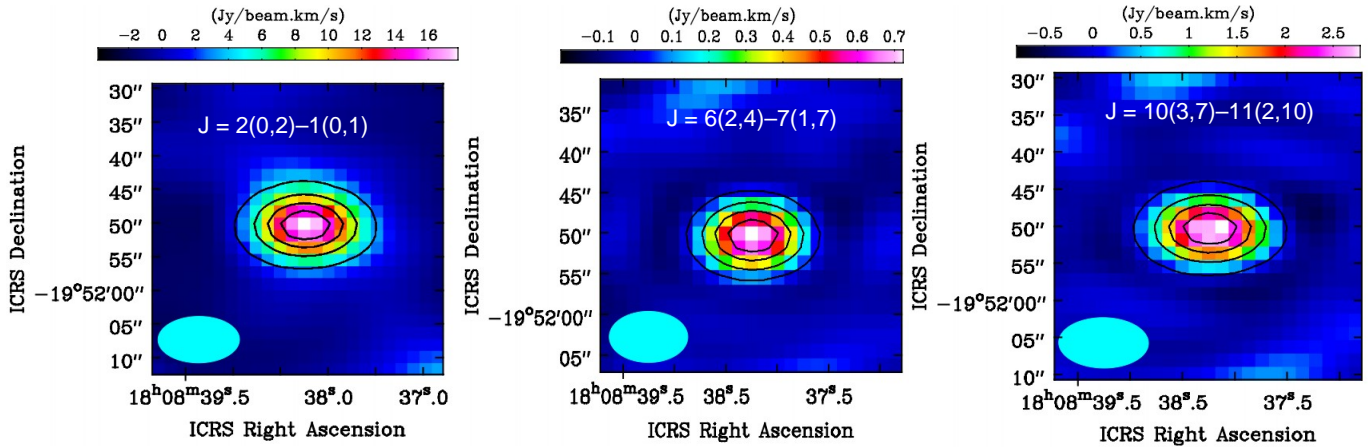


Fig. 5. Integrated emission maps of detected transitions of CH_2NH towards the G10.47+0.03, which are overlaid with the 2.34 mm continuum emission map. The contour levels are 20%, 40%, 60%, and 80% of peak flux. The cyan circle represents the synthesized beam of the integrated emission maps.

of the detected transitions vary between 9 K and 240 K. From the spatial distribution analysis, we estimated that the emission regions of CH_2NH vary between $10.520''$ – $10.781''$. The estimated molecular column density of CH_2NH towards G10.47+0.03 using the ACA was $(3.40 \pm 0.2) \times 10^{15} \text{ cm}^{-2}$ with a rotational temperature of 218.70 ± 20 K. Earlier, Suzuki et al. (2016) estimated that the column density of CH_2NH towards G10.47+0.03 using the NRO telescope is $(4.70 \pm 1.6) \times 10^{15} \text{ cm}^{-2}$ with a rotational temperature of 84 ± 57 K. We find that our estimated column density of CH_2NH is similar to that reported by Suzuki et al. (2016), but the temperature is different. The estimated rotational temperature of CH_2NH by Suzuki et al. (2016) indicates that the detected transition lines of CH_2NH arise from the cold region of G10.47+0.03. Our estimated temperature indicates that the emission lines of CH_2NH arise from the warm-inner region of G10.47+0.03. Suzuki et al. (2016) found the lower rotational temperature due to the lower spatial and spectral resolution of the NRO telescope. Our estimated higher excitation temperature of CH_2NH using ACA is accurate because the temperature of the hot molecular cores is above 100 K (van Dishoeck & Blake, 1998). The other two precursors of $\text{NH}_2\text{CH}_2\text{COOH}$, such as CH_3NH_2 (Ohishi et al., 2019) and $\text{NH}_2\text{CH}_2\text{CN}$ (Manna & Pal, 2022a) were also detected towards G10.47+0.03 using the NRO and ALMA telescopes. The detection of CH_2NH towards G10.47+0.03 indicates that three possible precursors of $\text{NH}_2\text{CH}_2\text{COOH}$ are present in G10.47+0.03. That means the hot molecular core G10.47+0.03 is an ideal candidate for searching the emission lines of $\text{NH}_2\text{CH}_2\text{COOH}$.

4.2. Comparison with modelled and observed abundance of CH_2NH

After estimating the fractional abundance of CH_2NH towards G10.47+0.03, we compared the estimated abundance of CH_2NH with the modelled abundance of CH_2NH , which was estimated from the two-phase warm-up chemical model (Suzuki et al., 2016). For chemical modelling, Suzuki et al. (2016) used the gas-grain chemical kinetics code NAUTILUS in an environment with hot molecular cores. In chemical modelling, Suzuki et al. (2016) assumed an isothermal collapse phase after a static warm-up phase. In the first phase, the gas density rapidly increased from 3×10^3 to $1 \times 10^7 \text{ cm}^{-3}$, and under free-fall collapse, the dust temperature decreased from 16 to 8 K. In the second phase, the gas density remained constant at $1 \times 10^7 \text{ cm}^{-3}$ and the gas temperature fluctuated rapidly from 8 K to 400 K (Suzuki et al., 2016). In chemical modelling, Suzuki et al. (2016) used the neutral-neutral reaction between CH_3 and NH radicals in the gas phase and the neutral-neutral reaction between CH_2 and NH radicals on the grain surface to create CH_2NH under the condition of hot molecular cores. The gas temperature of G10.47+0.03 was ~ 150 K (Rolffs et al., 2011) and the gas density was $7 \times 10^7 \text{ cm}^{-3}$ (Rolffs et al., 2011). Therefore, the two-phase warm-up chemical model of Suzuki et al. (2016), which is based on the time scale, is appropriate for explaining the chemical abundance and evolution of CH_2NH towards G10.47+0.03. After the simulation, Suzuki et al. (2016) observed that the modelled abundance of CH_2NH varied between $\sim 10^{-9}$ – 10^{-8} in the gas phase. Similarly, the abundance of CH_2NH on the grain surface is $\leq 10^{-12}$. We found that the abundance of CH_2NH towards the G10.47+0.03 is 2.61×10^{-8} , which is nearly similar to the modelled abundance of CH_2NH in the gas phase derived by Suzuki et al. (2016). This result indicates that CH_2NH was created towards G10.47+0.03, via the gas-phase neutral-neutral reaction between CH_3 and NH radicals.

Previously, Manna & Pal (2022a) claimed that $\text{NH}_2\text{CH}_2\text{CN}$ was the daughter molecule of CH_2NH (see Figure 1). The identification of both CH_2NH and $\text{NH}_2\text{CH}_2\text{CN}$ indicates that G10.47+0.03 is an ideal candidate in the ISM, where $\text{NH}_2\text{CH}_2\text{COOH}$ may exist. In ISM, G10.47+0.03 is the only source where the maximum number of possible $\text{NH}_2\text{CH}_2\text{COOH}$ precursors (such as NH_2CN , H_2CO , CH_3NH_2 , CH_2NH , and $\text{NH}_2\text{CH}_2\text{CN}$) is detected, and several prebiotic chemistries have been proposed to understand the possible formation mechanism of these molecules and their possible connection with $\text{NH}_2\text{CH}_2\text{COOH}$. After detecting the maximum number of $\text{NH}_2\text{CH}_2\text{COOH}$ precursors towards G10.47+0.03, we created a possible chemical network to understand the prebiotic chemistry of $\text{NH}_2\text{CH}_2\text{COOH}$ towards G10.47+0.03. The chemical network is shown in Figure 6. In the chemical network, all reactions were obtained from Woon et al. (2002); Theule et al. (2011); Danger et al. (2011); Garrod (2013); Alonso et al. (2018); Ohishi et al. (2019); Manna & Pal (2022a) and UMIST 2012 astrochemistry molecular reaction databases. The chemical network clearly indicates the maximum

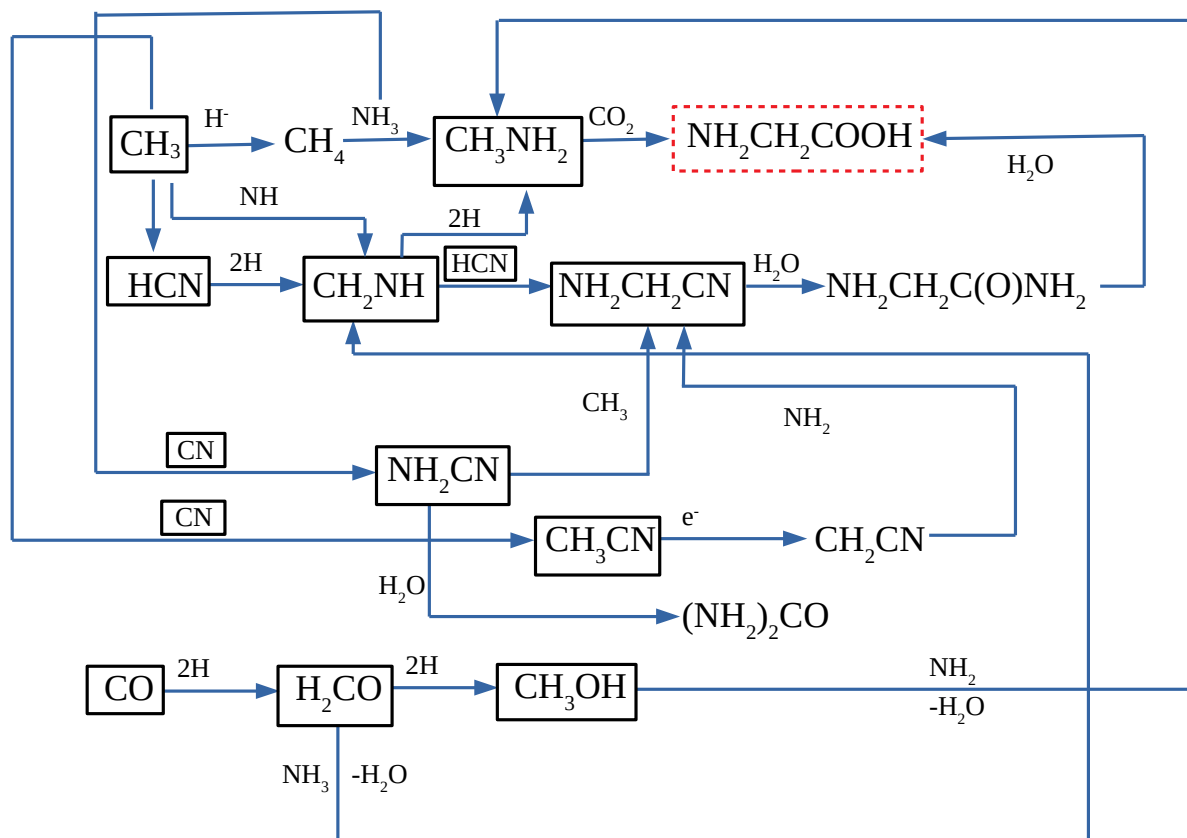


Fig. 6. Proposed chemical network for the formation of $\text{NH}_2\text{CH}_2\text{COOH}$ from other molecules. In the network, the red box molecule is the final daughter molecule ($\text{NH}_2\text{CH}_2\text{COOH}$) and the black box molecules are the parent molecules that are detected towards G10.47+0.03.

number of parent molecules detected towards G10.47+0.03, which gives us an idea about the chemical complexity towards hot molecular cores.

4.3. Searching of $\text{NH}_2\text{CH}_2\text{COOH}$ towards the G10.47+0.03 using the ACA

After the identification of three possible $\text{NH}_2\text{CH}_2\text{COOH}$ precursor molecules like CH_2NH (present paper), CH_3NH_2 (Ohishi et al., 2019), and $\text{NH}_2\text{CH}_2\text{CN}$ (Manna & Pal, 2022a) towards the G10.47+0.03, we searched the emission lines of $\text{NH}_2\text{CH}_2\text{COOH}$ conformers I and II towards the G10.47+0.03. After the careful spectral analysis using the LTE model, we did not detect any evidence of $\text{NH}_2\text{CH}_2\text{COOH}$ conformers I and II towards the G10.47+0.03 within the limits of our LTE modelling. The estimated upper limit column density of $\text{NH}_2\text{CH}_2\text{COOH}$ conformers I and II towards G10.47+0.03 was $\leq 1.02 \times 10^{15} \text{ cm}^{-2}$ and $\leq 2.36 \times 10^{13} \text{ cm}^{-2}$ respectively. The energy of $\text{NH}_2\text{CH}_2\text{COOH}$ conformer I is 705 cm^{-1} (1012 K) lower than that of $\text{NH}_2\text{CH}_2\text{COOH}$ conformer II (Lovas et al., 1995). The dipole moments of $\text{NH}_2\text{CH}_2\text{COOH}$ conformer I are $\mu_a = 0.911 \text{ D}$ (a-type) and $\mu_b = 0.607 \text{ D}$ (b-type), whereas $\text{NH}_2\text{CH}_2\text{COOH}$ conformer II has dipole moments of $\mu_a = 5.372 \text{ D}$ (a-type) and $\mu_b = 0.93 \text{ D}$ (b-type) (Lovas et al., 1995). In ISM, the detection of a-type^c transitions of $\text{NH}_2\text{CH}_2\text{COOH}$ are expected compared to b-type transitions because the line intensity of the molecule is proportional to the square of the dipole moments (Lovas et al., 1995). The detection of three possible $\text{NH}_2\text{CH}_2\text{COOH}$ precursor molecules towards G10.47+0.03 gives more confidence about the presence of $\text{NH}_2\text{CH}_2\text{COOH}$ towards G10.47+0.03.

5. Conclusion

In this article, we present the identification of the possible $\text{NH}_2\text{CH}_2\text{COOH}$ precursor molecule CH_2NH towards G10.47+0.03, using the ACA band 4. The main conclusions of this study are as follows:

1. We successfully identified three non-blended transition lines of CH_2NH towards the G10.47+0.03 using the ACA observation.
2. The estimated column density of CH_2NH towards G10.47+0.03 is $(3.40 \pm 0.2) \times 10^{15} \text{ cm}^{-2}$ with a rotational temperature of $218.70 \pm 20 \text{ K}$. The estimated fractional abundance of CH_2NH towards the G10.47+0.03 with respect to H_2 is 2.61×10^{-8} .

^cThe a-type and b-type are the different transitions of $\text{NH}_2\text{CH}_2\text{COOH}$, whose spectral parameters depend on the different electric dipole moments.

3. We compare the estimated abundance of CH₂NH with the two-phase warm-up chemical model abundance of CH₂NH proposed by Suzuki et al. (2016). We noticed that the modelled abundance of CH₂NH is nearly similar to the observed abundance of CH₂NH towards G10.47+0.03. This comparison indicates that CH₂NH is created via a gas-phase neutral-neutral reaction between CH₃ and NH radicals towards G10.47+0.03.

4. After the successful detection of CH₂NH towards G10.47+0.03, we also search the emission lines of the simplest amino acid NH₂CH₂COOH conformers I and II towards G10.47+0.03. We do not detect the emission lines of NH₂CH₂COOH conformers I and II within the limits of LTE modelling. The estimated upper-limit column densities of NH₂CH₂COOH conformers I and II are $\leq 1.02 \times 10^{15} \text{ cm}^{-2}$ and $\leq 2.36 \times 10^{13} \text{ cm}^{-2}$ respectively.

5. The unsuccessful detection of NH₂CH₂COOH towards G10.47+0.03 using ACA indicate that the emission lines of NH₂CH₂COOH may be below the confusion limit in G10.47+0.03.

Acknowledgement. We thank the anonymous referees for their helpful comments, which improved the manuscript. A.M. acknowledges the Swami Vivekananda merit cum means scholarship (SVMCM), Government of West Bengal, India, for financial support for this research. The plots within this paper and other findings of this study are available from the corresponding author upon reasonable request. This paper makes use of the following ALMA data: ADS/JAO.ALMA#2016.2.00005.S. ALMA is a partnership of ESO (representing its member states), NSF (USA), and NINS (Japan), together with NRC (Canada), MOST and ASIAA (Taiwan), and KASI (Republic of Korea), in co-operation with the Republic of Chile. The Joint ALMA Observatory is operated by ESO, AUI/NRAO, and NAOJ.

Conflicts of interest

The authors declare no conflict of interest.

References

- Alonso, E. R., Kolesníková, L., Białkowska-Jaworska, E., Kisiel, Z., León, I., Guillemin, J. C., Alonso, J. L., 2018, Glycinamide, a Glycine Precursor, Caught in the Gas Phase: A Laser-ablation Jet-cooled Rotational Study, *Astrophysical Journal*, 861, 70
- Allen, V., van der Tak, F. F. S., Sánchez-Monge, Á., Cesaroni, R., Beltrán, M. T., 2017, Chemical Segregation in Hot Cores With Disk Candidates: An investigation with ALMA, *Astronomy & Astrophysics*, 603, A133
- Bögelund, E. G., McGuire, B. A., Hogerheijde, M. R., van Dishoeck, E. F., Ligterink, N. F. W., 2019, Methylamine and other simple N-bearing species in the hot cores NGC 6334I MM1-3, *Astronomy & Astrophysics*, 624, A82
- Belloche, A., Müller, H. S. P., Menten, K. M., Schilke, P., & Comito, C., 2013, Complex organic molecules in the interstellar medium: IRAM 30 m line survey of Sagittarius B2(N) and (M), *Astronomy & Astrophysics*, 559, A47
- Cesaroni, R., Hofner, P., Araya, E., & Kurtz, S. 2010, The structure of hot molecular cores over 1000 AU, *Astronomy & Astrophysics*, 509, A50
- Dickens, J. E., Irvine, W. M., Devries, C. H., & Ohishi, M. 1997, Hydrogenation of Interstellar Molecules: A Survey for Methylenimine (CH₂NH), *Astrophysical Journal*, 479, 312
- Danger, G., et al., 2011, Experimental investigation of aminoacetonitrile formation through the Strecker synthesis in astrophysical-like conditions: reactivity of methanimine (CH₂NH), ammonia (NH₃), and hydrogen cyanide (HCN), *Astronomy & Astrophysics*, 535, A47
- Garrod, R. T. 2013, A Three-phase Chemical Model of Hot Cores: The Formation of Glycine, *Astrophysical Journal*, 765, 60
- Garrod, R. T., & Herbst, E. 2006, Formation of methyl formate and other organic species in the warm-up phase of hot molecular cores, *Astronomy & Astrophysics*, 457, 927
- Garrod, R. T., Jin, M., Matis, K. A., Jones, D., Willis, E. R., Herbst, E., 2022, Formation of Complex Organic Molecules in Hot Molecular Cores through Nondiffusive Grain-surface and Ice-mantle Chemistry, *Astrophysical Journal Supplement*, 259, 1
- Godfrey, P. D., Brown, R. D., Robinson, B. J., & Sinclair, M. W. 1973, Discovery of Interstellar Methanimine (Formaldimine), *Astrophysical Letters*, 13, 119
- Goldsmith, P. F., & Langer, W. D. 1999, Population Diagram Analysis of Molecular Line Emission, *Astrophysical Journal*, 517, 209
- Gorski, M. D., Aalto, S., Mangum, J., et al. 2021, Discovery of methanimine (CH₂NH) megamasers toward compact obscured galaxy nuclei, *Astronomy & Astrophysics*, 654, A110
- Halfen, D. T., Ilyushin, V. V., & Ziurys, L. M. 2013, Insights into Surface Hydrogenation in the Interstellar Medium: Observations of Methanimine and Methyl Amine in Sgr B2(N), *Astrophysical Journal*, 767, 66
- Herbst, E., & van Dishoeck, E. F. 2009, Complex Organic Interstellar Molecules, *Annual Review of Astronomy and Astrophysics*, 47, 427
- Jones, P. A., Burton, M. G., Cunningham, M. R., et al. 2008, Spectral imaging of the Sagittarius B2 region in multiple 3-mm molecular lines with the Mopra telescope, *Monthly Notices of the Royal Astronomical Society*, 386, 117
- Jones, P. A., Burton, M. G., Tothill, N. F. H., & Cunningham, M. R. 2011, Spectral imaging of the Sagittarius B2 region in multiple 7-mm molecular lines, *Monthly Notices of the Royal Astronomical Society*, 411, 2293
- Joshi, P. R. & Lee, Y. P. 2022, A chemical link between methylamine and methylene imine and implications for interstellar glycine formation, *Communications Chemistry*, 5, 62
- Kirchhoff, W.H., Johnson, D.R. Lovas, F.J., 1973, Microwave Spectra of Molecules of Astrophysical Interest: II Methylenimine, *Journal of Physical and Chemical Reference Data*, 2, 1
- Kurtz, S., Cesaroni, R., Churchwell, E., Hofner, P., & Walmsley, C. M. 2000, Hot Molecular Cores and the Earliest Phases of High-Mass Star Formation, *Protostars and Planets IV*, 299
- Lovas, F. J., Kawashima, Y., Grabow, J. U., Suenram, R. D., Fraser, G. T., Hirota, E., 1995, Microwave Spectra, Hyperfine Structure, and Electric Dipole Moments for Conformers I and II of Glycine, *Astrophysical Journal*, 455, L201

- Ligterink, N. F. W., Calcutt, H., Coutens, A., Kristensen, L. E., Bourke, T. L., Drozdovskaya, M. N., Müller, H. S. P., Wampfler, S. F., van der Wiel, M. H. D., van Dishoeck, E. F., Jørgensen, J. K., 2018, The ALMA-PILS survey: Stringent limits on small amines and nitrogen-oxides towards IRAS 16293-2422B, *Astronomy & Astrophysics*, 619, A28
- Manna, A., Pal, S., 2022a, Identification of interstellar amino acetonitrile in the hot molecular core G10.47+0.03: Possible glycine survey candidate for the future, *Life Sciences in Space Research*, 34, 9
- Manna, A., Pal, S., 2022b, Detection of interstellar cyanamide (NH₂CN) towards the hot molecular core G10.47+0.03 *Journal of Astrophysics and Astronomy*, 43, 83
- Manna, A., Pal, S., 2022c, First detection of methyl formate in the hot molecular core IRAS 18566+0408, *Astrophysics and Space Science*, 367, 94
- Manna, A., Pal, S., 2023a, Detection of complex nitrogen-bearing molecule ethyl cyanide towards the hot molecular core G10.47+0.03, *Astrophysics and Space Science*, 368, 44
- Manna, A., Pal, S., 2023b, Detection of monothioformic acid towards the solar-type protostar IRAS 16293–2422, *Journal of Astrophysics and Astronomy*, 44, 69
- Manna, A., Pal, S., Viti, S., Sinha, S., 2023, Identification of the simplest sugar-like molecule glycolaldehyde towards the hot molecular core G358.93–0.03 MM1, *Monthly Notices of the Royal Astronomical Society*, 525, 2229-2240
- Manna, A., Pal, S., 2024a, Detection of possible glycine precursor molecule methylamine towards the hot molecular core G358.93–0.03 MM1, *New Astronomy*, 109, 102199
- Manna, A., Pal, S., 2024b, ACA observation and chemical modeling of phosphorus nitride towards hot molecular cores G10.47+0.03 and G31.41+0.31, *Journal of Astrophysics and Astronomy*, 45, 3
- Manna, A., Pal, S., 2024c, Detection and Chemical Modeling of Complex Prebiotic Molecule Cyanamide in the Hot Molecular Core G31.41+0.31, *ACS Earth and Space Chemistry*, <https://doi.org/10.1021/acsearthspacechem.3c00245>
- Müller H. S. P., Schlemmer F., Stutzki J. Winnewisser G., 2005, The Cologne Database for Molecular Spectroscopy, CDMS: a useful tool for astronomers and spectroscopists, *Journal of Molecular Structure*, 742, 215
- McMullin, J. P., Waters, B., Schiebel, D., Young, W., & Golap, K. 2007, CASA Architecture and Applications, Astronomical Society of the Pacific Conference Series, Vol. 376, *Astronomical Data Analysis Software and Systems XVI*, ed. R. A. Shaw, F. Hill, & D. J. Bell, 127
- Ohishi, M., Suzuki, T., Hirota, T., Saito, M. Kaifu, N., Detection of a new methylamine (CH₃NH₂) source: Candidate for future glycine surveys, 2019, *Publications of the Astronomical Society of Japan*, 71, 86
- Perley, R. A., Butler, B. J. 2017, An Accurate Flux Density Scale from 50 MHz to 50 GHz, *Astrophysical Journal*, 230, 1538
- Qin, S.-L., Wu, Y., Huang, M., et al. 2010, High-Resolution Submillimeter Multiline Observations of G19.61-0.23: Small-Scale Chemistry, *Astrophysical Journal*, 711, 399
- Rivilla V. M., Beltrán M. T., Cesaroni R., et al. 2017, Formation of ethylene glycol and other complex organic molecules in star-forming regions, *Astronomy & Astrophysics*, 598, A59
- Rolfs, R., Schilke, P., Zhang, Q., & Zapata, L. 2011, Structure of the hot molecular core G10.47+0.03, *Astronomy & Astrophysics*, 536, A33
- Shimonishi, T., Izumi, N., Furuya, K., & Yasui, C., 2021, The Detection of a Hot Molecular Core in the Extreme Outer Galaxy, *Astrophysical Journal*, 2, 206
- Sanna, A., Reid, M. J., Menten, K. M., et al. 2014, Trigonometric parallaxes to star-forming regions within 4 kpc of the galactic center, *Astrophysical Journal*, 781, 108
- Suzuki, T., Ohishi, M., Hirota, T., Saito, M., Majumdar, L., Wakelam, V., 2016, Survey Observations of a Possible Glycine Precursor, Methanimine (CH₂NH), *Astrophysical Journal*, 825, 79
- Sutton, E. C., Jaminet, P. A., Danchi, W. C., & Blake, G. A. 1991, Molecular Line Survey of Sagittarius B2(M) from 330 to 355 GHz and Comparison with Sagittarius B2(N), *Astrophysical Journal Supplement*, 77, 255
- Tan, J. C., Beltrán, M. T., Caselli, P., et al. 2014, Massive Star Formation, Protostars and Planets VI, 149
- Theule, P., Borget, F., Mispelaer, F., Danger, G., Duvernay, F., Guillemin, J. C., Chiavassa, T., 2011, Hydrogenation of solid hydrogen cyanide HCN and methanimine CH₂NH at low temperature, *Astronomy & Astrophysics*, 534, A64
- Turner, B. E. 1989, A Molecular Line Survey of Sagittarius B2 and Orion-KL from 70 to 115 GHz. I. The Observational Data, *Astrophysical Journal Supplement*, 70, 539
- van Dishoeck E. F., & Blake G. A. 1998, Chemical Evolution of Star-Forming Regions, *Annual Review of Astronomy and Astrophysics*, 36, 317
- Vastel, C., Bottinelli, S., Caux, E., Glorian, J. -M., Boiziot, M., 2015, CASSIS: A TOOL TO VISUALIZE AND ANALYSE INSTRUMENTAL AND SYNTHETIC SPECTRA, Proceedings of the Annual meeting of the French Society of Astronomy and Astrophysics, 313-316
- Woon, D. E., 2002, Pathways to Glycine and Other Amino Acids in Ultraviolet-irradiated Astrophysical Ices Determined via Quantum Chemical Modeling, *Astrophysical Journal*, 571, L177
- White, G. J., Araki, M., Greaves, J. S., Ohishi, M., & Higginbottom, N. S. 2003, A spectral survey of the Orion Nebula from 455–507 GHz, *Astronomy & Astrophysics*, 407, 589